Research Square

Preprints are preliminary reports that have not undergone peer review.
They should not be considered conclusive, used to inform clinical practice,
or referenced by the media as validated information.

Labile Zinc Dynamics Trigger an Oxidative Cascade and Systemic Physiological Reorganization in Tribolium Castaneum

Liliana Ataides Silva Barichello
Goiano Federal Institute
Thiarlen Marinho Luz
Goiano Federal Institute
Rafaela Ribeiro Brito
Goiano Federal Institute
Bárbara Beatriz Silva Nunes
Goiano Federal Institute
Wesley Rodrigues Soares
Goiano Federal Institute
Nayeli Leticia Cortés Acevedo
Universidad de Guanajuato
Teresa de Jesús Monserrat López Estrada
Universidad de Guanajuato
Nancy Priscila Ayala Mejía
Universidad de Guanajuato
Ana Marlen Acosta Sierra
Universidad de Guanajuato
Aline Sueli de Lima Rodrigues
Goiano Federal Institute
Omar Cruz Santiago
Universidad de Guanajuato
Guilherme Malafaia#
guilherme.malafaia@ifgoiano.edu.br

Goiano Federal Institute

Research Article

Keywords: nanomaterials, terrestrial insects, oxidative stress, metal bioavailability, biochemical networks, ecotoxicology

Posted Date: May 20th, 2026

DOI: https://doi.org/10.21203/rs.3.rs-9349103/v1

License: This work is licensed under a Creative Commons Attribution 4.0 International License.
Read Full License

Additional Declarations: No competing interests reported.

Abstract

The expanding use of metallic nanomaterials in industrial, agricultural, and pharmaceutical applications has increased the environmental release of nanoparticles, among which zinc oxide nanoparticles (ZnO NPs) stand out not only for their wide range of applications but also for environmental concerns. Although the number of studies addressing their toxicity has grown considerably, most investigations have focused primarily on insecticidal effects or on the evaluation of isolated biomarkers, which limits the understanding of the integrated physiological mechanisms underlying the responses of non-target organisms to these materials. In this context, we investigated the effects of dietary exposure to ZnO NPs in adult *Tribolium castaneum*, examining the temporal dynamics of zinc bioavailability and its repercussions across multiple physiological axes. We exposed insects to two dietary concentrations of ZnO NPs (0.05% and 0.2%) for 120 h and performed assessments at different exposure times (12–120 h). We quantified biomarkers associated with the redox, metabolic, digestive, and neurochemical axes, as well as labile/extractable Zn concentrations and mortality. Our results showed that exposure to ZnO NPs initially increased the bioavailable Zn fraction in the organisms, followed by activation of an oxidative cascade characterized by elevated reactive oxygen species, lipid peroxidation, and modulation of antioxidant enzymes. We also observed subsequent alterations in metabolic and digestive pathways, including changes in total protein, soluble carbohydrate, and digestive enzyme activities, as well as neurochemical modulation of dopamine and serotonin. Integrated analyses based on the area under the curve and correlation networks further revealed that higher ZnO NP concentrations induced greater cumulative physiological divergence and a transient reorganization of the organisms' biochemical architecture, indicating systemic integration of the responses to the stressor. Taken together, our findings demonstrate that exposure to ZnO NPs triggers a hierarchical sequence of physiological events initiated by the mobilization of bioavailable Zn and culminating in a multisystem reorganization of insect physiology, thereby expanding the mechanistic understanding of the ecotoxicological effects of these nanomaterials in terrestrial non-target insects.

1. INTRODUCTION

Although zinc is an essential micronutrient involved in numerous structural, catalytic, and regulatory processes (Vallee & Auld, 1990; Andreini et al., 2006; Maret, 2013), its nano-structured form exhibits distinct physicochemical properties, such as high specific surface area, enhanced reactivity, and dynamic dissolution behavior, resulting in patterns of bioavailability that differ substantially from those of conventional ionic or bulk zinc forms (Nel et al., 2006; Handy et al., 2008; Ma et al., 2013; Amin & Erfan, 2025). In this sense, the exponential expansion of nanotechnology over the past two decades has led to the widespread incorporation of metallic nanomaterials into industrial, agricultural, pharmaceutical, and cosmetic production chains, thereby substantially increasing the potential environmental release of these particles across different ecological compartments (Pawar & Takke, 2023; Mekuye & Abera, 2023; Al-Harbi et al., 2025). Among these materials, zinc oxide nanoparticles (ZnO NPs) stand out due to their broad range of applications, including antimicrobial activity, photocatalytic properties, thermal stability, and ultraviolet radiation absorption (Lebaka et al., 2025;

Espitia et al., 2025; Yang et al., 2025; Ragu-Prasath & Selvam, 2025). Consequently, ZnO NPs can reach both aquatic and terrestrial ecosystems through multiple release pathways, including industrial effluents, sewage sludge, fertilizers, and veterinary products, thereby constituting a continuous source of environmental input (Beegam et al., 2016; Rajput et al., 2018; Sun et al., 2023; Kang et al., 2024).

Experimental studies conducted over the past decade have shown that exposure to ZnO NPs can induce adverse effects at multiple levels of biological organization. For instance, Kool et al. (2011)investigated the chronic toxicity of ZnO NPs, non-nano ZnO, and $ZnCl_2$ in *Folsomia candida*. They observed that although survival remained unaffected even at high concentrations (6400 mg Zn kg^{-1}), reproductive capacity was significantly reduced, suggesting that toxic effects might be associated with the release of Zn^{2+} ions in the environment. In another study, Mekiwi et al. (2012) evaluated the insecticidal activity of ZnO NPs synthesized by thermal decomposition of zinc acetate in a cross-linked polyacrylic acid polymer matrix against *Galleria mellonella*. They reported pronounced larval mortality in a dose- and time-dependent manner, along with the appearance of intermediate larva–pupa forms and adults with malformed or reduced wings, indicating direct interference with metamorphosis. Subsequently, Abd El-Wahab and Anwar (2014), when testing ZnO NPs in *Spodoptera litura*, recorded complete mortality (100%) at a dose of 0.01 g, increased apoptotic cells in hemocytes after 24 h of exposure, and reduced activity of antioxidant enzymes such as ascorbate peroxidase and superoxide dismutase, indicating disruption of the redox system. Further evidence of acute toxicity across different insect orders was provided by Khooshe-Bast et al. (2016), who demonstrated high toxicity of hexagonal ZnO NPs (wurtzite structure) in *Trialeurodes vaporariorum*, reporting an LC_{50} of 7.35 mg L^{-1} and mortality reaching 91.6% at the highest concentration tested.

Studies conducted with dipterans have likewise documented the toxicity of both commercially produced ZnO NPs and particles obtained through green synthesis routes. Examples include investigations using commercial ZnO NPs in *Drosophila melanogaster* (Alaraby et al., 2015), *Culex pipiens* (Ibrahim et al., 2023), and *Culex quinquefasciatus* (Ahluwalia et al., 2023). Other studies have evaluated nanoparticles synthesized or functionalized with biological extracts. Among these are ZnO NPs encapsulated with herbal extracts (Banumathi et al., 2017) and ZnO NPs synthesized using aqueous extract of *Ulva lactuca* L. (Abinaya et al., 2018), both tested against *Aedes aegypti*. Additional examples include ZnO NPs coated with exopolysaccharides from *Bacillus licheniformis* Dahb1 evaluated in *Aedes stephensi* (Ishwarya et al., 2018), ZnO NPs functionalized with *Lobelia leschenaultiana* tested in *Lucilia sericata* (Banumathi et al., 2018), ZnO NPs synthesized from *Anabasis articulata* assessed in *Aedes aegypti* (Alamri et al., 2024), ZnO NPs derived from *Eucalyptus globulus* also evaluated in *Aedes aegypti* (Majeed et al., 2024), and ZnO NP formulations biocapsulated with essential oils investigated in larvae of *Lucilia sericata* (Çelik et al., 2025).

Despite the consistency of these findings, most studies conducted with insects have predominantly focused on the insecticidal potential of ZnO NPs, examining these particles mainly from the perspective of their application in the control of agricultural pests or disease vectors and, consequently, overlooking their ecotoxicological implications for non-target organisms. In addition, many of these investigations

have been restricted to the assessment of isolated toxicity biomarkers, which limits our understanding of the physiological mechanisms linking the bioavailability of zinc released by nanoparticles to the biological responses observed in exposed organisms. Another recurrent methodological aspect is the evaluation of effects at a single time point, typically at the end of the experimental period, without considering the temporal dynamics of biological responses following exposure. This limitation is particularly relevant because the toxicological effects of nanomaterials may follow non-linear trajectories over time, involving compensatory responses, physiological acclimation processes, or delayed effects that remain undetected in single-point assessments. In this context, experimental approaches capable of integrating multiple biomarkers across time and assessing the functional reorganization of the biological system in a systemic manner remain scarce in the literature. The development of analytical strategies of this nature is therefore essential for advancing the mechanistic understanding of ZnO NP toxicity in non-target insects, especially considering that these nanomaterials may reach different environmental compartments and ecological niches, potentially triggering integrated physiological disturbances that culminate in adverse effects in exposed organisms.

Within this framework, we aimed to investigate the physiological and biochemical effects of exposure to ZnO NPs in *Tribolium castaneum*, evaluating the temporal dynamics of Zn bioavailability and their potential repercussions across multiple physiological axes, including oxidative, metabolic, digestive, and neurochemical responses. Specifically, we tested the hypothesis that exposure to ZnO NPs increases labile Zn concentrations within organisms, potentially influencing biomarkers associated with redox balance, energy metabolism, digestion, and neurochemistry. Additionally, we hypothesized that these responses may occur in an integrated manner over time, resulting in detectable changes in the overall biomarker profile and in the relationships among physiological variables.

2. MATERIAL AND METHODS

2.1. Zinc oxide nanoparticles

The ZnO nanoparticles (ZnO NPs) used in this study were commercially obtained (Sigma-Aldrich, St. Louis, MO, USA; CAS 544906) and had been previously characterized by our research group (Souza et al., 2018), showing > 99.99% purity, no surface coating, and a mean primary diameter of 68.96 ± 33.71 nm. Transmission electron microscopy and X-ray diffraction analyses confirmed a polygonal morphology and a wurtzite-type crystalline structure with no detectable impurities. In aqueous suspensions, ZnO NPs formed aggregates with hydrodynamic diameters of 445.75 ± 13.72 nm in MQ water and 431.4 ± 13.83 nm in dechlorinated water, low polydispersity indices (0.235 ± 0.023 and 0.257 ± 0.010), and surface charges of 25.33 ± 0.79 mV and − 18.4 ± 0.52 mV, respectively (Motta et al., 2020).

2.2. Model system and experimental design

We used adults of *Tribolium castaneum* (Coleoptera: Tenebrionidae) of both sexes as the model system, representing non-target insects potentially exposed to metallic nanoparticles in environments associated with grain and food storage. The insects were obtained from laboratory colonies maintained

in the Terrestrial Organism Vivarium of the Laboratory of Applied Environmental Toxicology (Instituto Federal Goiano – Urutaí Campus, GO, Brazil). The organisms presented an average body mass of 2.08 ± 0.11 mg (mean ± SD) and were selected to ensure similar body size and the absence of visible morphological abnormalities. To evaluate the effects of exposure to ZnO NPs, organisms were distributed into three experimental groups, each comprising 30 replicates of 30 individuals, totaling 900 insects per group.

The control group consisted of *T. castaneum* maintained on a standard dietary substrate based on whole wheat flour without nanoparticle supplementation. The ZnONP-I and ZnONP-II groups were maintained under the same experimental conditions, but with the dietary substrate supplemented with ZnO NPs at proportions of 0.05% (500 mg kg^{-1}) and 0.2% (2000 mg kg^{-1}) (w/w), respectively. The lower concentration (ZnONP-I) was defined as an estimated sublethal experimental level, with effects previously reported in terrestrial invertebrates (Hilal et al., 2021; Maryum et al., 2024; Singh et al., 2025), whereas the higher concentration (ZnONP-II) was included to represent an experimental scenario of increased exposure intensity. Moreover, the selection of these concentrations followed a hazard-based mechanistic approach aimed at inducing measurable physiological responses without causing widespread acute mortality, thereby allowing us to investigate how exposure to ZnO NPs modulates different physiological axes over time. Due to the aggregation behavior of nanoparticles in aqueous media at the concentrations required for dietary supplementation, we incorporated ZnO NPs directly as dry nanopowder. For this purpose, the corresponding mass of nanoparticles was first weighed on an analytical balance, distributed over the surface of the dry dietary substrate, and subsequently homogenized, following procedures similar to those described by Hooper et al. (2011) and Singh et al. (2025).

All groups were maintained in glass containers (5 cm diameter × 10.5 cm height) covered with nonwoven fabric membranes, allowing ventilation while preventing the escape of organisms. The containers were kept in a climatic chamber at 27°C under constant darkness, following the conditions described by Herren et al. (2025) and Malafaia et al. (2025). Experimental assessments were performed at 12, 24, 48, 72, 96, and 120 h of exposure, time points defined to capture both early physiological responses and delayed effects resulting from ZnO NP exposure over the experimental period. To achieve this, we adopted a destructive sampling scheme in which independent replicates were removed at each time point, ensuring statistical independence among samples (Underwood, 1997; Quinn & Keough, 2002). At each experimental time, five replicates per group were removed from the experiment. Each replicate consisted of a container holding 30 individuals and was considered the experimental unit for subsequent analyses. After removal, the organisms were weighed and immediately processed for the subsequent analyses.

2.3. Determination of labile/extractable zinc

To preferentially quantify the biologically available fraction of Zn, potentially resulting from the dissolution or biotransformation of ZnO NPs after internalization by the organisms, rather than the total metal content associated with different cellular compartments, we determined concentrations of

labile/extractable Zn, considered a proxy of the redox-active and potentially bioavailable fraction of the metal. For this purpose, random pools of *T. castaneum* obtained from each replicate (n = 10–14 individuals) were weighed and homogenized in PBS buffer (pH 7.2) using a cell disruptor. The homogenate was subsequently centrifuged (13,000 rpm, 10 min, 4°C) and filtered through 0.45 µm syringe filters. Quantification of labile/extractable Zn was performed using a colorimetric method adapted from Sharma and Amlathe (2012), based on the reaction between Zn^{2+} ions present in the supernatant and a mixture containing potassium hexacyanoferrate (III) and diphenylamine, which results in the formation of a green chromophore whose intensity is proportional to the concentration of available Zn in the sample. In 96-well microplates, we added 100 µL of a 3.5% potassium hexacyanoferrate(III) solution, 100 µL of a 0.25% diphenylamine solution, 5 µL of the sample supernatant, and 5 µL of purified water. To correct for potential matrix effects, a second aliquot of the same sample was treated with 5 µL of a Zn standard solution ($ZnCl_2$, equivalent to 1000 µg Zn mL^{-1}), while PBS was used as the blank. After homogenization, absorbance was measured in a microplate reader at 630 nm. Extractable Zn concentrations were estimated by comparing readings from samples with and without standard addition, considering the dilution factor of the assay, and the results were expressed as µg Zn mg^{-1} biomass.

2.4. Toxicity biomarkers

To evaluate the physiological effects resulting from exposure to ZnO NPs, we adopted several integrated biochemical parameters as toxicity biomarkers, in addition to mortality rate, calculated as the proportion of dead individuals relative to the initial number of organisms in each replicate. For biochemical analyses, random pools of *T. castaneum* from each replicate (n = 10–14 individuals) were also weighed and processed as described above. The resulting supernatant was used for subsequent analyses and stored at -80°C until use.

The redox axis was characterized by biomarkers associated with the organisms' oxidative and antioxidant responses at each evaluation time and treatment. Reactive oxygen species (ROS) levels were quantified using a method based on 2',7'-dichlorofluorescein-diacetate (DCF-DA) (Zhao et al., 2013), and malondialdehyde (MDA) levels, a marker of lipid peroxidation, were determined through the reaction with 1-methyl-2-phenylindole (MPI) (Islayem et al., 2022). The activities of the antioxidant enzymes superoxide dismutase (SOD) and catalase (CAT) were determined according to Das et al. (2000) and Hadwan and Abed (2016), respectively. Additionally, we evaluated esterase activity using *p*-nitrophenyl butyrate (pNPB) as substrate (Kim et al., 2024) and glutathione S-transferase (GST) activity using 1-chloro-2,4-dinitrobenzene (CDNB) as substrate (Vontas et al., 2000). Nitrite (NO_2^-) levels, the main stable metabolite of nitric oxide, were determined using the Griess reaction (Grisham et al., 1996). Total thiols were also quantified using the Ellman method (Ellman, 1959), employing the reagent 5,5'-dithiobis-(2-nitrobenzoic acid) (DTNB), and were considered a proxy for the availability of free sulfhydryl groups (–SH) involved in detoxification processes and in the regulation of Zn bioavailability in exposed organisms.

Within the neurochemical axis, serotonin levels were determined based on the reaction with ammonium metavanadate in acidic medium (Pathak et al., 1979), and dopamine levels were quantified through

reaction with ceric ammonium nitrate in the presence of 3,3',5,5'-tetramethylbenzidine under acidic conditions (Liang et al., 2021; Wang et al., 2017). Within the metabolic axis, we determined total protein levels using a commercial colorimetric kit (Biotécnica®, Ref. 10.009.00, based on the reaction between cupric ions and peptide bonds), triglycerides using an enzymatic-colorimetric kit (Biotécnica®, Ref. 10.010.00), based on the generation of hydrogen peroxide from glycerol-3-phosphate oxidation), and total soluble carbohydrates determined by the phenol–sulfuric acid method (DuBois et al., 1956). Finally, within the digestive axis, we determined the activities of the proteases trypsin and chymotrypsin using a spectrophotometric assay with fluorogenic substrate (FITC-casein) (Twining, 1984), as well as lipase activity using *p*-nitrophenyl palmitate as a chromogenic substrate (Yel et al., 2021).

2.5. Data analysis

2.5.1. Univariate analyses

We initially sought to determine whether exposure to different ZnO NP concentrations and exposure times promoted individual changes in the evaluated biomarkers, and whether such effects occurred independently or interactively. To this end, biomarkers were assessed for normality and homogeneity of variances using the Shapiro–Wilk and Levene tests, respectively. When necessary, appropriate transformations (e.g., log or log1p) were applied to meet parametric assumptions. Analyses were conducted with two fixed factors: experimental group (Control, NP-I, and NP-II) and exposure time (12, 24, 48, 72, 96, and 120 h), including the interaction term group × time. Depending on the fulfillment of assumptions and the distribution of residuals, we employed two-way ANOVA, two-way ANOVA on transformed data, or ART-ANOVA (aligned rank transform) when parametric assumptions could not be adequately satisfied. When main effects or interactions were significant, multiple comparisons were performed using Tukey's test. The significance level adopted was $\alpha = 0.05$. All statistical analyses were performed in the R environment (R Core Team), mainly using the packages stats, car, ARTool, rstatix, and emmeans, whereas the final graphical representations were produced in GraphPad Prism v10.4.2.

2.5.2. Trajectory divergence and cumulative burden estimation

To evaluate the integrated response over time, we calculated the area under the curve (AUC) for each biomarker across the entire experimental period (12–120 h) using the trapezoidal method. AUC values were estimated from group means at each time point. To allow comparisons among biomarkers measured on different scales, AUC values were standardized using a z-score transformation. The cumulative deviation relative to the control group was expressed as ΔAUC, calculated as the difference between the treatment AUC and the corresponding control AUC. These analyses were performed in the R environment (R Core Team) using the dplyr and tidyr packages.

2.5.3. Lag-Based modeling of the oxidative cascade

To investigate potential directional temporal relationships within the oxidative cascade, we adopted a lag-based modeling approach in the R environment (R Core Team). For each experimental group, the

mean concentration of labile extractable Zn from the immediately preceding time point was calculated and assigned to observations at the subsequent time point, establishing a 24 h lag structure and generating a treatment-specific predictor (Zn_prev_mean). Linear models fitted by ordinary least squares (function lm) were used to test (i) the association between lagged labile Zn and ROS levels through the model *ROS ~ group × Zn_prev_mean*, and (ii) subsequent associations between ROS and oxidative damage or antioxidant response markers (e.g., MDA, SOD, CAT, and NO) using interaction models (*response ~ group × ROS*). Analyses were restricted to time points for which lagged values were available (24–120 h). Model assumptions of normality, homoscedasticity, and goodness-of-fit were evaluated through graphical inspection of residuals and standard diagnostic procedures. Main effects and interactions were examined using analysis of variance (function anova), and effect size was estimated using partial eta squared (ηp^2), calculated as SS_effect/(SS_effect + SS_residual). Overall model fit was summarized using the adjusted coefficient of determination (R^2_adj) and the global F statistic. Data organization and preprocessing were performed using the dplyr package.

2.5.4. Integrated deviation analysis and standardized temporal profiling

To evaluate the integrated temporal dynamics of oxidative biomarkers (ROS, MDA, SOD, CAT, and NO) and enable direct comparison among variables originally measured on different scales, we performed a Z-score–based standardization using the control group distribution as the reference. First, the mean and standard deviation of each biomarker were estimated considering only the control individuals. Subsequently, individual values from the exposed groups (ZnONP-I and ZnONP-II) were transformed into standardized scores, expressing deviations in standard deviation units relative to the control group. We then calculated mean scores for each group × time × biomarker combination, allowing the construction of comparable temporal profiles across variables. Values outside this range were retained through scale compression (squish function from the scales package), preventing visual distortion or the generation of missing values. All analyses and visualizations were conducted in the R environment using the dplyr, tidyr, ggplot2, viridis, and scales packages.

2.5.5. Correlation network construction and global topological analysis of biochemical system dynamics

Finally, to characterize the structural reorganization of the biochemical system as a whole, we performed a correlation network analysis constructed separately for each group × time combination (Control, NP-I, and NP-II; 12–120 h). For each subset, we estimated a correlation matrix among quantitative variables after verifying univariate normality using the Shapiro–Wilk test. As most distributions did not show significant deviations from normality ($p > 0.05$), Pearson correlation coefficients were calculated. Networks were defined as undirected weighted graphs, with edge weights corresponding to the absolute values of the correlation coefficients. No significance threshold was applied to preserve the system's complete interaction structure. Topological analyses were conducted in the R environment using the igraph package. Global network metrics extracted included number of nodes (vcount), number of edges

(ecount), network density (edge_density), mean nodal strength and its standard deviation (strength), weighted clustering coefficient (transitivity, type = "weighted"), structural modularity based on the Louvain algorithm (cluster_louvain followed by modularity), and global efficiency, estimated as the mean inverse geodesic distance between all pairs of nodes. These metrics were organized using the dplyr package and, for comparative purposes across time points and treatments, were standardized by z-score transformation within each metric.

3. RESULTS

Initially, our results showed that mortality was significantly influenced by the experimental group (χ^2 = 15.66; $p < 0.001$), exposure time (χ^2 = 14.64; $p = 0.012$), and the interaction between these factors (χ^2 = 24.91; $p = 0.0055$), according to a binomial GLM with logit link function (Fig. 1A). At the early time points (12–24 h), mortality rates remained low, and no clear differences among groups were observed. However, at 48 h of exposure, we detected a significant increase in mortality in the ZnONP-II group, corresponding to an absolute increase of 8 percentage points (≈ 602% relative increase). In contrast, no differences among groups were observed at 72 h and 96 h. The highest mortality peak occurred at 120 h, when the ZnONP-II group exhibited mortality approximately seven times that observed in the NP-I group (2.66%) and 18.66 percentage points higher than the control group (0%) (Fig. 1A).

Regarding labile/extractable Zn concentrations, two-way ANOVA revealed significant effects of group ($F = 10.78$; $p < 0.001$), exposure time ($F = 43.71$; $p < 0.001$), and the group × time interaction ($F = 8.10$; $p < 0.001$), indicating that intergroup differences varied depending on the temporal point evaluated. As shown in Fig. 1B, after 24 h of exposure, animals treated with ZnO NPs exhibited significantly higher concentrations than the control group, with increases of 113.9% (ZnONP-I) and 147.8% (ZnONP-II). In subsequent evaluations, comparisons among groups within each time point revealed an oscillatory pattern in the ZnONP-II group, with concentrations lower than the control at 48 h, higher at 72 h, again lower at 96 h, and no significant difference at 120 h, indicating concentration-dependent temporal modulation. In the same group, 24 h after the peak Zn concentration observed at 24 h, we detected, at 48 h, a tendency toward a 48.6% increase in total thiol levels relative to the control group. In contrast, no clear differences among groups were observed in subsequent evaluations. This pattern suggests a transient response possibly associated with intracellular redistribution of the metal and its binding to molecules with high affinity for sulfhydryl groups (Fig. 1C).

<Insert Fig. 1**>**

Regarding oxidative biomarkers, two-way ANOVA revealed a significant effect of exposure time for all evaluated variables (ROS, MDA, SOD, and CAT; Figs. 2A–D, respectively), whereas the group factor alone was significant only for CAT. We also observed a significant group × time interaction for ROS and CAT, indicating that the temporal trajectories of these biomarkers were modulated by exposure to ZnO NPs. Notably, at the 48 h evaluation, 24 h after the maximum peak of labile/extractable Zn concentrations was detected in the ZnONP-II group, we observed significantly higher ROS levels in this group, with an

average increase of 31.3% relative to the other groups. This increase was accompanied by a concomitant elevation in MDA levels, SOD and CAT activities, and nitrite concentrations, thereby configuring a coordinated activation of the redox axis. The hypothesis of a cascade-like organization underlying this pattern was further supported by sequential modeling (Table 1), which demonstrated that the association between lagged labile Zn and ROS was treatment-dependent and that, under higher exposure intensity, the association was stronger. ROS levels explained a substantial portion of the variation observed in downstream biomarkers of the oxidative cascade, with the largest effect size detected for SOD, followed by MDA, NO, and CAT. The hierarchy of these effects is summarized in Fig. 2G, which illustrates the functional organization of the redox axis under ZnO NP exposure.

Table 1
Sequential models testing the lagged association between labile/extractable Zn and the hierarchical activation of the oxidative cascade in *Tribolium castaneum* exposed to ZnO nanoparticles.

Model (Response)	**Effect**	**F-values**	**p-values**	**Partial η²**
ROS (group × Zn_prev_mean model)	Group	0.664	0.518	0.019
	Zn_prev_mean	0.269	0.606	0.004
	Group × Zn_prev_mean	6.736	0.002	0.163
MDA (group × ROS model)	Group	3.126	0.050	0.083
	ROS	21.910	< 0.0001	0.241
	Group × ROS	0.472	0.626	0.014
SOD (group × ROS model)	Group	2.149	0.124	0.059
	ROS	58.691	< 0.0001	0.459
	Group × ROS	0.602	0.551	0.017
CAT (group × ROS model)	Group	0.807	0.450	0.023
	ROS	11.642	0.0011	0.144
	Group × ROS	0.141	0.869	0.004
NO (group × ROS model)	Group	7.294	0.0013	0.175
	ROS	14.448	0.00031	0.173
	Group × ROS	0.879	0.420	0.025

<Insert Fig. 2 **and** Table 1**>**

Regarding metabolic biomarkers, we observed that total protein showed a significant effect of the group factor ($F = 3.94$; $p = 0.0238$), with an increase exceeding 15% in the ZnONP-II group relative to the control, indicating exposure-dependent modulation across all evaluated time points (Fig. 3A). In contrast, triglyceride levels were significantly influenced by exposure time ($F = 16.62$; $p < 0.0001$), revealing an

increasing temporal trend, with higher values observed at 72 h, 96 h, and 120 h (Fig. 3B), without an isolated effect of group or a significant interaction. For total soluble carbohydrates, we detected significant effects of group ($F = 4.41$; $p = 0.0156$) and time ($F = 6.76$; $p < 0.0001$), as well as a significant group × time interaction ($F = 2.83$; $p = 0.0051$), indicating that the temporal dynamics of this variable differed among treatments (Fig. 3C). Specifically, in the intergroup comparison performed at 120 h, the ZnONP-II group exhibited TSC levels approximately 30% lower than those of the control group. Additionally, at the 48 h evaluation, the pronounced increases observed in the ZnONP-II group for total proteins, triglycerides, and TSC coincided with the peak lipase activity detected in this same group (Fig. 3D), as well as with significant differences relative to the control in the activities of digestive proteases (trypsin and chymotrypsin), which were approximately 35% higher than the control at that time point (Figs. 3E–F, respectively).

<Insert Fig. 3**>**

Conversely, dopamine levels measured at 24 h were lower in the ZnONP-II group than in the control group (Fig. 4A). Considering the significant interaction between group and time, this result indicates that the neurochemical response depended on the temporal dynamics of exposure and did not remain linear across the subsequent evaluation periods. Regarding 5-HT levels, although the two-way ANOVA indicated a significant effect only on exposure time, we observed a tendency toward a 23.91% reduction at 120 h in the ZnONP-II group relative to the control, suggesting a possible late treatment-specific effect (Fig. 4B).

<Insert Fig. 4**>**

Beyond the differences observed at specific time points and considering the significant interaction between group and time for several biomarkers, we also evaluated the cumulative response across the entire experimental period to identify which treatment produced the greatest overall physiological deviation. For the above, we used the area under the curve (AUC) of each biomarker as an integrated measure of response over time. Our analysis revealed that the ZnONP-II group exhibited the greatest cumulative divergence relative to the control across most evaluated biomarkers, indicating a broader and more systemic physiological reorganization throughout the experiment (Table 2). Specifically, more pronounced positive cumulative deviations were observed for total proteins, nitrite, and digestive proteases ($\Delta AUC_z > 68$), indicating sustained increases in these responses over time. In contrast, relevant negative cumulative deviations were detected for SOD activity, esterases, and dopamine levels ($\Delta AUC_z < -31$), suggesting a persistent reduction in these parameters under ZnO NP exposure, particularly in the ZnONP-II group (Fig. 5).

Table 2
Standardized cumulative physiological divergence (ΔAUC⧠) of biomarkers in *Tribolium castaneum* adults following dietary exposure to ZnO nanoparticles over the 120-h experimental period.

Biomarker	**Physiological axis**	**ΔAUC⧠ (ZnONP-I)**	**ΔAUC⧠ (ZnONP-II)**	**Greater divergence**
Total proteins	Metabolic	33.2	102.0	ZnONP-II
Nitrite (NO)	Oxidative/Redox	21.3	96.5	ZnONP-II
Lipase	Digestive	79.6	-5.54	ZnONP-I
Chymotrypsin	Digestive	19.5	77.0	ZnONP-II
Trypsin	Digestive	16.4	68.2	ZnONP-II
MDA	Oxidative/Redox	27.4	60.2	ZnONP-II
Total soluble carbohydrates	Metabolic	59.6	20.7	ZnONP-I
Esterases	Digestive	-23.4	-49.4	ZnONP-II
Triglycerides	Metabolic	8.47	47.8	ZnONP-II
Dopamine	Neurochemical	24.1	-45.3	ZnONP-II
Total thiols	Oxidative/Redox	-2.97	36.8	ZnONP-II
SOD	Oxidative/Redox	-17.7	-31.8	ZnONP-II
GST	Detoxification	-6.51	19.6	ZnONP-II
Serotonin (5-HT)	Neurochemical	19.2	3.54	ZnONP-I
ROS	Oxidative/Redox	-8.07	-14.2	ZnONP-II
CAT	Oxidative/Redox	10.3	-13.4	ZnONP-II

Note: ΔAUC⧠ represents the standardized cumulative deviation from the control group across the experimental period (12–120 h), calculated from the area under the curve (AUC) of each biomarker time-series and expressed as z-standardized differences relative to the control trajectory. Positive ΔAUC⧠ values indicate sustained upregulation, whereas negative values indicate persistent suppression relative to the control condition. ZnONP-I and ZnONP-II correspond to diets supplemented with low and high concentrations of ZnO nanoparticles, respectively. Abbreviations: ROS – reactive oxygen species; MDA – malondialdehyde; SOD – superoxide dismutase; CAT – catalase; GST – glutathione S-transferase; NO – nitric oxide (measured as nitrite); 5-HT – serotonin.

<Insert Fig. 5 **and** Table 2**>**

Finally, analysis of the biochemical network architecture revealed structural changes that depend on both treatment and exposure time, as reflected in connectivity metrics among the evaluated biomarkers. In the ZnONP-II group, particularly at 72 h, we observed a pronounced increase in the number of connections (n = 136), accompanied by maximum network density, the highest mean degree (16), a

global clustering coefficient equal to 1.000, and a peak in mean interaction strength (mean strength = 12.506) (Table 3 and Fig. 6), defining the point of greatest systemic integration throughout the experiment. Z-score standardization further corroborated this pattern by identifying 72 h as a structural inflection point specific to this group, characterized by a simultaneous increase in global efficiency and connection intensity, accompanied by a reduction in modularity, consistent with a transient reorganization of the biochemical response under higher exposure intensity (Fig. 7). In contrast, the control group exhibited gradual variation over time, maintaining relatively stable network density and clustering but showing a progressive increase in mean connection strength, reaching a maximum at 120 h (mean strength = 10.706), suggesting intensification of correlations without structural reconfiguration of the network. The ZnONP-I group, in turn, displayed only minor oscillations in connectivity metrics and did not reach the level of integration observed in the ZnONP-II group at 72 h.

Table 3
Temporal changes in the topology and connectivity of biochemical interaction networks in *Tribolium castaneum* exposed to ZnO nanoparticles.

Group	Time (h)	Number of nodes	Number of connections	Network density	Mean degree	Clustering coefficient	Mean connection strength
Control	12	17	131	0.963	15.412	0.964	6.897
	24	17	129	0.949	15.176	0.948	8.317
	48	17	129	0.949	15.176	0.947	6.824
	72	17	131	0.963	15.412	0.962	6.929
	96	17	129	0.949	15.176	0.947	7.565
	120	17	131	0.963	15.412	0.967	10.706
ZnONP-I	12	17	129	0.949	15.176	0.945	6.976
	24	17	130	0.956	15.294	0.953	6.882
	48	17	129	0.949	15.176	0.95	7.765
	72	17	129	0.949	15.176	0.947	7.235
	96	17	132	0.971	15.529	0.97	7.165
	120	17	126	0.926	14.824	0.923	6.685
ZnONP-II	12	17	129	0.949	15.176	0.953	6.961
	24	17	132	0.971	15.529	0.97	8.271
	48	17	131	0.963	15.412	0.961	7.188
	72	17	136	1.000	16.000	1.000	12.506
	96	17	130	0.956	15.294	0.957	6.635
	120	17	133	0.978	15.647	0.979	8.652

Note. Networks were constructed from pairwise correlations among biochemical biomarkers measured in adult *T. castaneum* at each exposure time. Nodes represent individual biomarkers included in the analysis, whereas connections (edges) represent pairwise correlations between biomarkers, with edge weights equal to the absolute value of the correlation coefficient (|r|). No significance threshold was applied in order to preserve the full interaction structure of the biochemical system. Network density indicates the proportion of observed connections relative to the maximum possible number of connections for a network with the same number of nodes. Mean degree represents the average number of connections per node, reflecting overall network connectivity. The clustering coefficient quantifies the tendency of interconnected biomarkers to form locally clustered groups within the network. Mean connection strength corresponds to the average magnitude of the association weights (|r|) across all edges, reflecting the overall intensity of biochemical coupling among biomarkers.

<Insert Figs. 6–7 **and** Table 3**>**

4. DISCUSSION

Our results demonstrate that dietary exposure to ZnO NPs triggers in adult *T. castaneum* a complex and temporally structured physiological response, characterized by sequential alterations that begin with an increase in the bioavailable fraction of Zn and progressively evolve into a systemic reorganization involving multiple physiological axes. Overall, the higher exposure scenario (ZnONP-II) produced the most pronounced alterations, as evidenced both by the increase in mortality at later time points and by the greater cumulative physiological deviation observed in the evaluated biomarkers. More importantly, the results indicate that these alterations did not occur in isolation but followed a temporal trajectory, with an initial increase in labile Zn, elevated ROS levels, activation of antioxidant biomarkers, and, subsequently, metabolic, digestive, and neurochemical changes. This pattern suggests that metal bioavailability acts as an initial trigger, initiating a cascade of integrated physiological responses and reinforcing the hypothesis that the effects of ZnO NPs emerge from the dynamic interaction among metal dissolution processes, redox perturbations, and systemic metabolic reorganization.

More specifically, the initial increase in labile Zn concentrations observed within the first 24 h of exposure is consistent with the physicochemical behavior described for ZnO NPs in complex physiological matrices, in which these particles may undergo surface dissolution and release biologically available Zn^{2+} ions. Several studies indicate that ZnO NPs exhibit a strong tendency toward surface dissolution, releasing Zn^{2+} ions that subsequently contribute to the bioavailable metal fraction within the exposed organism (Lv et al., 2012; Ma et al., 2013; Yung et al., 2017; Lenaka et al., 2025; Alprol et al., 2026). In this context, the increase of up to 147.8% in extractable Zn observed in our study (Fig. 1B) suggests that exposure to ZnO NPs(whether through direct ingestion or through adhesion to body surfaces, particularly the cuticle, with possible indirect ingestion during grooming) promoted rapid mobilization of the metal within the organisms. In contrast, the oscillatory dynamics observed at subsequent time points likely reflect physiological processes involved in regulating metal homeostasis, including intracellular sequestration, redistribution among cellular compartments, and binding to molecules rich in sulfhydryl groups. The tendency toward increased total thiol levels following the Zn peak (Fig. 1C) supports this interpretation, as compounds containing –SH groups play a fundamental role in regulating metal bioavailability and protecting against toxicity associated with excess metal ions (Maret, 2013). Thus, the data indicates that exposure to ZnO NPs initially disrupts zinc homeostasis, followed by compensatory mechanisms aimed at restoring intracellular metal balance.

The subsequent activation of the redox axis observed in this study provides additional evidence that the increase in Zn bioavailability constitutes an upstream event capable of triggering oxidative responses in *T. castaneum* exposed to ZnO NPs. The significant increase in ROS observed 24 h after the Zn peak, accompanied by elevated MDA levels, increased SOD and CAT activities, and higher nitrite concentrations (Fig. 2), indicates the coordinated activation of oxidative damage and antioxidant defense processes. This pattern is consistent with the toxicity mechanism frequently associated with metallic nanoparticles, in which redox imbalance is a key mediator of the biological effects of these particles across different experimental models (Rajput et al., 2018; Kang et al., 2024). The sequential

modeling adopted in this study (Table 1) further supports this interpretation by demonstrating that variation in ROS levels explained a substantial portion of the variation observed in downstream biomarkers of the oxidative cascade, particularly for SOD activity and MDA levels. From a mechanistic perspective, this process may involve both the direct interaction of ZnO NPs with cellular components, an interpretation supported by in vitro studies demonstrating cytotoxicity, oxidative damage, and genomic alterations in cells exposed to nanoparticles (Shen et al., 2013; Ng et al., 2017), and the disruption of redox homeostasis associated with the release of Zn^{2+} ions, which can alter the activity of metal-dependent enzymes and compromise the stability of proteins sensitive to redox status.

Beyond oxidative responses, exposure to ZnO NPs also promoted changes in the metabolic and digestive axes, suggesting that the effects of these particles extend beyond oxidative stress alone. The increase in digestive enzyme activities observed at specific experimental time points (Figs. 3D–F), together with the concomitant elevation of total proteins, triglycerides, and soluble carbohydrates (Figs. 3A–C), suggests a reorganization of energy metabolism in the exposed organisms. In biological systems, metabolic changes of this nature are consistent with compensatory responses aimed at maintaining homeostasis under stress conditions, since detoxification processes, cellular repair, and antioxidant defenses tend to reconfigure energy allocation, with measurable consequences for nutrient consumption, assimilation efficiency, and digestive enzymatic profiles (Seyed-Alian et al., 2024). The temporal coincidence between increases in digestive enzyme activities and peaks in metabolic biomarkers therefore suggests that exposure to nanoparticles may induce intensified nutrient assimilation and reconfiguration of the energetic budget of exposed organisms, as demonstrated by Seyed-Alian et al. (2024) in a study with dietary nanomaterials in *Acheta domesticus*, in which digestive enzymes and parameters related to food consumption and assimilation were quantified simultaneously.

In parallel, the neurochemical alterations observed, particularly the transient reduction in dopamine levels (Fig. 4A), indicate that exposure to nanomaterials may also interfere with the nervous system's regulatory processes. As highlighted by Siju et al. (2021), in insects, dopamine acts as a central modulator of foraging and feeding decisions, as well as locomotion, suggesting that variations in its concentration may reflect broader physiological disturbances under stress conditions. Although we did not directly measure the activity of key enzymes involved in dopaminergic biosynthesis (e.g., tyrosine hydroxylase) or the integrity of dopaminergic neural circuits, it is plausible that the reduced dopamine levels observed in the ZnONP-II group, coinciding with the Zn peak, are related to interference of excess Zn with dopaminergic synthesis, given that evidence from *Drosophila melanogaster* indicates that Zn exposure can reduce dopamine levels and induce phenotypes consistent with dopaminergic dysfunction (Nadiga et al., 2025). On the other hand, the tendency toward a late reduction in 5-HT levels (120 h; Fig. 4B) may reflect a progressive alteration in serotonergic tone associated with nutritional status or prolonged physiological stress. As highlighted by Vleugels et al. (2015) and Banu et al. (2023), serotonin regulates, in a state-dependent manner, the microstructure of feeding behavior and the control of food intake in insects. In this context, although the increase in labile Zn was observed only during the early phases of exposure, it is plausible that the physiological disturbance initially triggered by ZnO NPs

promoted persistent metabolic and energetic adjustments over time, ultimately leading to late modulation of serotonergic signaling.

Conversely, the integrative analyses conducted in this study indicate that the effects of ZnO NPs were not restricted to isolated alterations in individual biomarkers but involved a systemic reorganization of the physiological architecture of the exposed organisms. The cumulative deviation analysis revealed that the treatment with the highest ZnO NP concentration produced the greatest overall physiological divergence relative to the control, simultaneously affecting multiple functional axes (Fig. 5 and Table 2). In addition, correlation network analysis (Figs. 6–7 and Table 3) demonstrated that exposure to ZnO NPs altered the connectivity structure among biomarkers, culminating in a peak of systemic integration observed at 72 h in the ZnONP-II group. This simultaneous increase in network density, mean degree, and interaction strength therefore suggests a transient reorganization of biochemical connectivity, possibly reflecting the coordinated activation of multiple physiological pathways in response to the stress imposed by the nanomaterials. Similar patterns of stress-induced physiological integration have been reported in adult *T. castaneum* exposed to other pollutants, such as microplastics (Malafaia et al., 2025; Guimarães et al., 2026). Although these contaminants act through physicochemical mechanisms distinct from those associated with ZnO NPs, both can trigger cellular disturbances that mobilize multiple physiological systems in an integrated manner. In such scenarios, different biochemical pathways may begin to operate more interdependently as part of an adaptive response to stress. In this context, the increased connectivity observed in our study may indicate the simultaneous activation of processes associated with energy metabolism, antioxidant defense, and detoxification, a phenomenon often interpreted as a temporary functional reorganization of the physiological system aimed at preserving homeostasis under environmental perturbation (Calabrese et al., 2007).

Taken together, our results indicate that dietary exposure to ZnO NPs can trigger in *T. castaneum* a hierarchical sequence of physiological events that begins with changes in metal bioavailability and progresses toward a systemic reorganization involving multiple functional axes. From an ecological perspective, these findings are particularly relevant because *T. castaneum* represents a detritivorous insect and a non-target organism potentially exposed to nanomaterials present in anthropogenically influenced terrestrial environments, including grain storage systems and compartments associated with decomposing organic matter. Physiological alterations such as those observed in our study may compromise fundamental processes related to energy metabolism, resource assimilation, and neurobehavioral regulation, with potential consequences for individual performance, survival, and reproductive success. At the ecological scale, disturbances of this nature in detritivorous insects may affect energy fluxes and organic matter cycling in terrestrial ecosystems, and potentially influence the transfer of contaminants along trophic chains. Furthermore, by integrating multiple biomarkers, temporal modeling, and biochemical network analysis, our study demonstrates that the toxicity of ZnO NPs may manifest as a dynamic systemic physiological reorganization that is difficult to detect with conventional ecotoxicological approaches based on a limited number of isolated endpoints. The results presented here therefore expand the mechanistic understanding of ZnO NP effects in terrestrial non-target insects and reinforce the need for integrative and multisystem approaches to achieve a more realistic

assessment of the ecological risks associated with the increasing environmental release of nanomaterials, in line with recommendations in the field of nanomaterial ecotoxicology that emphasize the importance of integrating multiple levels of biological response in the risk assessment of these emerging contaminants (Handy et al., 2012).

5. LIMITATIONS AND FUTURE DIRECTIONS

Although our study provides mechanistic evidence that dietary exposure to ZnO NPs can trigger an integrated temporal cascade (labile Zn → redox disturbance → metabolic–digestive reconfiguration → neurochemical modulation → systemic reorganization), several limitations should be acknowledged to guide interpretation and, more importantly, to inform future research directions. First, the tested concentrations were defined under a hazard-based rationale and therefore may not directly reflect typical environmental levels; consequently, ecological extrapolation should be approached with caution, and future studies should incorporate more environmentally realistic scenarios (including mixtures and environmental matrices) and chronic and multigenerational exposures. Second, although we quantified labile/extractable Zn as a proxy of bioavailability, we did not measure total body Zn, its distribution across tissues or compartments (e.g., gut, Malpighian tubules, and hemolymph), nor the speciation or transformation of particles along the digestive tract. In this regard, complementary approaches, such as ICP-MS for total Zn quantification, subcellular fractionation, microscopy coupled with energy-dispersive spectroscopy (EDS), and dissolution assays under simulated intestinal lumen conditions, could help distinguish between the “particulate” and “ionic” components of the observed responses. Finally, although we evaluated a broad set of biochemical biomarkers, we did not directly measure functional endpoints that are critical from an ecological and fitness perspective (e.g., food consumption and assimilation, locomotor or foraging behavior, fecundity, egg viability, and population performance). Consequently, the link between the physiological reorganization observed here and potential demographic consequences remains inferential and should be explicitly tested in future experimental designs.

6. CONCLUSIONS

In conclusion, our results demonstrate that dietary exposure to zinc oxide nanoparticles induces an integrated, time-dependent physiological response in adult *T. castaneum*, initiated by increased Zn bioavailability and followed by activation of the oxidative cascade, with subsequent repercussions across metabolic, digestive, and neurochemical axes. The integrated analysis of biomarkers, including temporal modeling, cumulative deviation analysis, and biochemical network architecture, revealed that the effects of ZnO NPs emerge as a systemic reorganization of organismal physiology, particularly under higher exposure intensity. This pattern indicates that initial disturbances in metal homeostasis may trigger redox responses that propagate across multiple biological systems, ultimately resulting in broad physiological changes potentially relevant to organismal performance. Thus, this study expands the mechanistic understanding of ZnO NP toxicity in terrestrial non-target insects and highlights that ecotoxicological assessments based on multisystem and temporally explicit approaches are essential

for achieving a more realistic understanding of the ecological risks associated with the increasing environmental release of nanomaterials.

Declarations

7. ACKNOWLEDGMENTS

The authors thank the National Council for Scientific and Technological Development (CNPq, Brazil) for financial support related to this research (process no. 308854/2021-7), which was essential for the successful development of this study. We also acknowledge the Coordination for the Improvement of Higher Education Personnel (CAPES, Brazil) for the doctoral scholarship granted to R.R. Brito and the Goiás State Research Foundation (FAPEG, Brazil) for the scholarship granted to T.M. Luz.

8. STATEMENTS AND DECLARATIONS

Ethical Approval: Although this study did not involve the use of vertebrate animals and is therefore not subject to mandatory evaluation by an Institutional Animal Care and Use Committee (IACUC) or an equivalent ethics board, all procedures were conducted by internationally recognized standards for the ethical treatment of invertebrates in scientific research. The experimental design followed the 3Rs principles (Replacement, Reduction, and Refinement) to minimize potential distress and ensure responsible animal handling. All efforts were made to reduce unnecessary manipulation and to maintain optimal environmental and husbandry conditions throughout the experimental period.

Consent to participate: Not applicable.

Consent to publish: Not applicable.

CRediT author statement:

Liliana Ataides Silva Barichello: Conceptualization, Methodology, Investigation, Validation, Visualization, Writing – Original Draft, and Writing - Review & Editing. **Thiarlen Marinho da Luz**: Conceptualization, Methodology, Investigation, Validation, Visualization, and Writing - Review & Editing. **Rafaela Ribeiro de Brito, Bárbara Beatriz da Silva Nunes, Wesley Rodrigues Soares, Nayeli Leticia Cortés Acevedo, Teresa de Jesús Monserrat López Estrada, Nancy Priscila Ayala Mejía, Ana Marlen Acosta Sierra**: Investigation, Validation, Visualization, Writing – Original Draft, and Writing - Review & Editing. **Aline Sueli de Lima Rodrigues and Omar Cruz Santiago**: Validation, Visualization, and Writing - Review & Editing. **Guilherme Malafaia**: Conceptualization, Methodology, Validation, Formal Analysis, Resources, Data Curation, Writing – Original Draft, Review and Editing, Supervision, Project Administration, Funding Acquisition

Competing interests: We confirm that there are no known conflicts of interest associated with this work, and that there has been no significant financial support that could have influenced its outcome. All listed authors have thoroughly read and approved the manuscript, and no other individuals meet the authorship criteria but are omitted. We emphasize that the peer review process is entirely under the responsibility of

the handling editor, who has full autonomy to select, invite, and assign qualified reviewers based on their scientific expertise and relevance to the topic. The editor also retains exclusive authority over all editorial decisions related to the manuscript's evaluation and potential publication. We reaffirm our commitment to upholding the highest ethical standards in scientific publishing and to ensuring an impartial, transparent, and rigorous review process.

Availability of data and materials: All data generated or analyzed during this study are included in this published article. Furthermore, the data supporting this study's findings are available on request from the corresponding author, [Malafaia G.].

Declaration of generative AI

In this study, we utilized artificial intelligence tools, specifically GPT-4, developed by OpenAI and accessed through the OpenAI platform. The GPT-4-turbo version was employed for linguistic enhancement and data processing, providing guidance on the necessary transformations to adapt the data and suggesting which statistical analyses would be most suitable to achieve the study's objectives. We ensured that the AI tool was used under strict human supervision.

References

1. Abd El-Wahab RA, Anwar EM (2014) The effect of direct and indirect use of nanoparticles on cotton leaf worm, *Spodoptera littoralis*. Int J Chem Biol Sci 1(7):17–24
2. Abinaya M, Vaseeharan B, Divya M, Sharmili A, Govindarajan M, Alharbi NS, Benelli G (2018) Bacterial exopolysaccharide (EPS)-coated ZnO nanoparticles showed high antibiofilm activity and larvicidal toxicity against malaria and Zika virus vectors. J Trace Elem Med Biol 45:93–103
3. Ahluwalia KK, Thakur K, Ahluwalia AS, Hashem A, Avila-Quezada GD, Abd_Allah EF, Thakur N (2023) Assessment of genotoxicity of zinc oxide nanoparticles using mosquito as test model. Toxics 11(11):887
4. Alamri AA, Alanazi NAH, Mashlawi AM, Shommo SA, Akeel MA, Alhejely A, Salama SA (2024) Chemical composition of Anabasis articulata, and biological activity of greenly synthesized zinc oxide composite nanoparticles (Zn-NPs): antioxidant, anticancer, and larvicidal activities. Agronomy 14(8):1742
5. Alaraby M, Annangi B, Hernández A, Creus A, Marcos R (2015) A comprehensive study of the harmful effects of ZnO nanoparticles using *Drosophila melanogaster* as an in vivo model. J Hazard Mater 296:166–174
6. Alprol AE, Hamad TM, Sharaf HE, El-Sayed HS, Barakat KM, Abouelwafa A, Khairy HM (2026) Toxicological impacts of biogenic zinc oxide nanoparticles on blue Parrotfish using multibiomarker assessment. Sci Rep 16(1):6546
7. Amin N, Erfan MA (2025) Environmental fate and toxicity of zinc oxide nanoparticles in aquatic ecosystems: A comprehensive review. J Nat Sci Rev 3(1):104–125

8. Andreini C, Banci L, Bertini I, Rosato A (2006) Zinc through the three domains of life. J Proteome Res 5(11):3173–3178
9. Banu A, Gowda SB, Salim S, Mohammad F (2023) Serotonergic control of feeding microstructure in Drosophila. Front Behav Neurosci 16:1105579
10. Banumathi B, Vaseeharan B, Ishwarya R, Govindarajan M, Alharbi NS, Kadaikunnan S, Benelli G (2017) Toxicity of herbal extracts used in ethno-veterinary medicine and green-encapsulated ZnO nanoparticles against Aedes aegypti and microbial pathogens. Parasitol Res 116(6):1637–1651
11. Banumathi B, Vaseeharan B, Malaikozhundan B, Ramasamy P, Govindarajan M, Alharbi NS, Benelli G (2018) Green larvicides against blowflies, *Lucilia sericata* (Diptera, Calliphoridae): Screening of seven plants used in Indian ethno-veterinary medicine and production of green-coated zinc oxide nanoparticles. Physiol Mol Plant Pathol 101:214–218
12. Beegam A, Prasad P, Jose J, Oliveira M, Costa FG (2016) Environmental Fate of Zinc Oxide Nanoparticles: Risks. *Toxicology: New aspects to this scientific conundrum*, 81
13. Calabrese EJ, Bachmann KA, Bailer AJ, Bolger PM, Borak J, Cai L, Mattson MP (2007) Biological stress response terminology: integrating the concepts of adaptive response and preconditioning stress within a hormetic dose–response framework. Toxicol Appl Pharmcol 222(1):122–128
14. Çelîk HT, Vural NİL, Ü. FER, Kaymak S (2025) Green synthesis and larvicidal activity of ZnO nanoparticles against Lucilia sericata larvae using essential oil bio-reductants. Vet Parasitol, 110633
15. Das K, Samanta L, Chainy GBN (2000) A modified spectrophotometric assay of superoxide dismutase using nitrite formation by superoxide radicals. Indian J Biochem Biophys 37:201–204
16. DuBois M, Gilles KA, Hamilton JK, Rebers PA, Smith F (1956) Colorimetric method for determination of sugars and related substances. Anal Chem 28(3):350–356
17. Ellman GL (1959) Tissue sulfhydryl groups. Arch Biochem Biophys 82(1):70–77
18. Eskin A, Nurullahoğlu ZU (2022) Effects of zinc oxide nanoparticles (ZnO NPs) on the biology of Galleria mellonella L.(Lepidoptera: Pyralidae). J Basic Appl Zool 83(1):54
19. Eskin A, Öztürk Ş, Körükçü M (2019) Determination of the acute toxic effects of zinc oxide nanoparticles (ZnO NPs) in total hemocytes counts of Galleria mellonella (Lepidoptera: Pyralidae) with two different methods. Ecotoxicology 28(7):801–808
20. Espitia PJP, Otoni CG, Soares NFF (2025) Zinc oxide nanoparticles for food packaging applications. Antimicrobial food packaging. Academic, pp 603–610
21. Grisham MB, Johnson GG, Lancaster JR Jr (1996) Quantitation of nitrate and nitrite in extracellular fluids. Methods in enzymology, vol 268. Academic, pp 237–246
22. Guimarães A, de Oliveira RF, de Souza Oliveira P, Barbosa KAD, de Lima Rodrigues AS, de Brito RR, Malafaia G (2026) A trophic bridge for bioplastic pollution: transstadial retention and systemic toxicity of polylactic acid microplastics from necrophagous flies (Chrysomya megacephala) to secondary consumer beetles (Tribolium castaneum). *Environ. Sci.: Processes Impacts, 2026,28, 431–456*

23. Hadwan MH, Abed HN (2016) Data supporting the spectrophotometric method for the estimation of catalase activity. Data brief 6:194–199
24. Handy RD, Cornelis G, Fernandes T, Tsyusko O, Decho A, Sabo-Attwood T, Horne N (2012) Ecotoxicity test methods for engineered nanomaterials: practical experiences and recommendations from the bench. Environ Toxicol Chem 31(1):15–31
25. Handy RD, Von der Kammer F, Lead JR, Hassellöv M, Owen R, Crane M (2008) The ecotoxicology and chemistry of manufactured nanoparticles. Ecotoxicology 17(4):287–314
26. Herren P, Svendsen C, Savio C, Meyling NV, Dunn AM, Hesketh H (2025) Double trouble? Quantifying the risk from co-exposure to multiple pathogens in Tenebrio molitor at different CO2 concentrations. J Invertebr Pathol 209:108269
27. Hilal SM, Mohmed AS, Barry NM, Ibrahim MH (2021), November Entomotoxicity of TiO2 and ZnO nanoparticles against adults tribolium castaneum (Herbest)(Coleoptera: Tenebrionidae). In *IOP conference series: earth and environmental science* (Vol. 910, No. 1, p. 012088). IOP Publishing
28. Hooper HL, Jurkschat K, Morgan AJ, Bailey J, Lawlor AJ, Spurgeon DJ, Svendsen C (2011) Comparative chronic toxicity of nanoparticulate and ionic zinc to the earthworm Eisenia veneta in a soil matrix. Environ Int 37(6):1111–1117
29. Ibrahim AM, Alfuhaid NA, Thabet MA, Ali AM (2023) Chronic effects induced by zinc oxide nanoparticles against larvae of the northern house mosquito *Culex pipiens (*Diptera: Culicidae). Int J Trop Insect Sci 43(6):1937–1945
30. Ishwarya R, Vaseeharan B, Kalyani S, Banumathi B, Govindarajan M, Alharbi NS, Benelli G (2018) Facile green synthesis of zinc oxide nanoparticles using Ulva lactuca seaweed extract and evaluation of their photocatalytic, antibiofilm and insecticidal activity. J Photochem Photobiol B 178:249–258
31. Islayem D, Fakih FB, Lee S (2022) Comparison of colorimetric methods to detect malondialdehyde, A biomarker of reactive oxygen species. ChemistrySelect, 7(11), e202103627
32. Kang M, Liu Y, Weng Y, Wang H, Bai X (2024) A critical review on the toxicity regulation and ecological risks of zinc oxide nanoparticles to plants. Environ Science: Nano 11(1):14–35
33. Khooshe-Bast Z, Sahebzadeh N, Ghaffari-Moghaddam M, Mirshekar A (2016) Insecticidal effects of zinc oxide nanoparticles and Beauveria bassiana TS11 on Trialeurodes vaporariorum (Westwood, 1856)(Hemiptera: Aleyrodidae). Acta Agriculturae Slov 107(2):299–309
34. Kim SH, Shin N, Jeon JM, Yoon JJ, Joo JC, Kim HT, Yang YH (2024) Application of liquid-based colorimetric method for high throughput screening of bioplastic-degrading strains using esterase assay. Anal Biochem 685:115390
35. Kool PL, Ortiz MD, van Gestel CA (2011) Chronic toxicity of ZnO nanoparticles, non-nano ZnO and ZnCl2 to Folsomia candida (Collembola) in relation to bioavailability in soil. Environ Pollut 159(10):2713–2719
36. Lebaka VR, Ravi P, Reddy MC, Thummala C, Mandal TK (2025) Zinc oxide nanoparticles in modern science and technology: multifunctional roles in healthcare, environmental remediation, and

industry. Nanomaterials 15(10):754

37. Liang L, Zhao Z, Ye F, Zhao S (2021) Rapid and sensitive colorimetric detection of dopamine based on the enhanced-oxidase mimicking activity of cerium (IV). New J Chem 45(15):6780–6786
38. Lv J, Zhang S, Luo L, Han W, Zhang J, Yang K, Christie P (2012) Dissolution and microstructural transformation of ZnO nanoparticles under the influence of phosphate. Environ Sci Technol 46(13):7215–7221
39. Ma H, Williams PL, Diamond SA (2013) Ecotoxicity of manufactured ZnO nanoparticles–a review. Environ Pollut 172:76–85
40. Ma H, Williams PL, Diamond SA (2013) Ecotoxicity of manufactured ZnO nanoparticles–a review. Environ Pollut 172:76–85
41. Malafaia G, Guimarães A, Soares WR, de Menezes IPP, de Lima Rodrigues AS, Gomes AR, da Luz TM (2025) Functional Reorganization and Systemic Toxicity Induced by Microplastics and Climate-Relevant Stressors in Tribolium Castaneum: Are We Simulating Tomorrow'S Toxic Reality? Environ Res, 122462
42. Maret W (2013) Zinc biochemistry: from a single zinc enzyme to a key element of life. Adv Nutr 4(1):82–91
43. Maryum A, Yasmin H, Saeed Q, Ahmed AM, Popescu SM, Ahmad F (2024) Phytofabrication and characterization of ZnO nanoparticles with Anagallis arvensis as promising eco-friendly insecticide against Tribolium castaneum Herbst. J King Saud University-Science 36(5):103162
44. Mekewi M, Shebl A, Imam AI, Amin MS, Albert T (2012) Screening the insecticidal efficacy of nano ZnO synthesized via in-situ polymerization of crosslinked polyacrylic acid as a template. J Mater Sci Technol 28(11):961–968
45. Mekuye B, Abera B (2023) Nanomaterials: An overview of synthesis, classification, characterization, and applications. Nano select 4(8):486–501
46. Motta AGC, Amaral do, Benvindo-Souza DF, Rocha M, T. L., e Silva DDM (2020) Genotoxic and mutagenic effects of zinc oxide nanoparticles and zinc chloride on tadpoles of Lithobates catesbeianus (Anura: Ranidae). Environ Nanatechnol Monit Manage 14:100356
47. Nadiga AP, Krishna KL, Moin A, Lila ASA, Rizvi SMD, Sahyadri M, Khafagy ES (2025) Exposure of Zinc-induced Parkinson's disease-like non-motor and motor symptoms in relation to oxidative/nitrosative stress mediated neurodegeneration in the brain of Drosophila melanogaster. J Pharmacol Sci 158(4):303–309
48. Nel A, Xia T, Madler L, Li N (2006) Toxic potential of materials at the nanolevel. Science 311(5761):622–627
49. Ng CT, Yong LQ, Hande MP, Ong CN, Yu LE, Bay BH, Baeg GH (2017) Zinc oxide nanoparticles exhibit cytotoxicity and genotoxicity through oxidative stress responses in human lung fibroblasts and Drosophila melanogaster. Int J Nanomed, 1621–1637
50. Pathak VN, Shukla C (1979) A new colorimetric method for determination of serotonine creatinine sulphate. Indian J Chem 8A:276–278

51. Pawar S, Takke A (2023) Regulatory aspects, types and bioapplications of metallic nanoparticles: a review. Curr Drug Deliv 20(7):857–883
52. Quinn GP, Keough MJ (2002) Experimental design and data analysis for biologists. Cambridge University Press
53. Ragu-Prasath A, Selvam K (2025) A review of the zinc oxide nanoparticles synthesis and their emerging biomedical potential. Biomedical Mater Devices, 1–25
54. Rajput VD, Minkina TM, Behal A, Sushkova SN, Mandzhieva S, Singh R, Movsesyan HS (2018) Effects of zinc-oxide nanoparticles on soil, plants, animals and soil organisms: A review. Environ Nanatechnol Monit Manage 9:76–84
55. Seyed-Alian R, Flasz B, Kędziorski A, Majchrzycki Ł, Augustyniak M (2024) Concentration-and time-dependent dietary exposure to graphene oxide and silver nanoparticles: effects on food consumption and assimilation, digestive enzyme activities, and body mass in Acheta domesticus. Insects 15(2):89
56. Sharma RD, Amlathe S (2012) Quantitative determination and removal of zinc using disposable colorimetric sensors: An appropriate alternative to optodes. J Chem Pharm Res 4(2):1097–1105
57. Shen C, James SA, de Jonge MD, Turney TW, Wright PF, Feltis BN (2013) Relating cytotoxicity, zinc ions, and reactive oxygen in ZnO nanoparticle–exposed human immune cells. Toxicol Sci 136(1):120–130
58. Siju KP, De Backer JF, Grunwald Kadow IC (2021) Dopamine modulation of sensory processing and adaptive behavior in flies. Cell Tissue Res 383(1):207–225
59. Singh K, Malla MA, Kumar A, Yadav S (2025) Comparative toxicity of zinc oxide nanoparticles and ionic zinc to earthworm Eudrilus eugeniae in Soil Matrix. Discover Soil 2(1):17
60. Sun H, Guo W, Zhou Q, Gong Y, Lv Z, Wang Q, Kopittke PM (2023) Uptake, transformation, and environmental impact of zinc oxide nanoparticles in a soil-wheat system. Sci Total Environ 857:159307
61. Twining SS (1984) Fluorescein isothiocyanate-labeled casein assay for proteolytic enzymes. Anal Biochem 143(1):30–34
62. Underwood AJ (1997) Experiments in ecology: their logical design and interpretation using analysis of variance. Cambridge University Press
63. Vallee BL, Auld DS (1990) Zinc coordination, function, and structure of zinc enzymes and other proteins. Biochemistry 29(24):5647–5659
64. Vleugels R, Verlinden H, Vanden Broeck J (2015) Serotonin, serotonin receptors and their actions in insects. *Neurotransmitter*, *2*
65. Vontas JG, Enayati AA, Small GJ, Hemingway J (2000) A simple biochemical assay for glutathione S-transferase activity and its possible field application for screening glutathione S-transferase-based insecticide resistance. Pestic Biochem Physiol 68(3):184–192

66. Wang HB, Li Y, Dong GL, Gan T, Liu YM (2017) A convenient and label-free colorimetric assay for dopamine detection based on the inhibition of the Cu (ii)-catalyzed oxidation of a 3, 3', 5, 5'-tetramethylbenzidine–H2O2 system. New J Chem 41(23):14364–14369
67. Yang J, Xiong D, Long M (2025) Zinc oxide nanoparticles as next-generation feed additives: Bridging antimicrobial efficacy, growth promotion, and sustainable strategies in animal nutrition. Nanomaterials 15(13):1030
68. Yel NV (2021) Investigation of the activity of lipase variants on different 4-nitrophenyl esters by spectrophotometric assay. Cauc J Sci 8(2):292–303
69. Yung MM, Kwok KW, Djurišić AB, Giesy JP, Leung KM (2017) Influences of temperature and salinity on physicochemical properties and toxicity of zinc oxide nanoparticles to the marine diatom Thalassiosira pseudonana. Sci Rep 7(1):3662
70. Zhao X, Wang S, Wu Y, You H, Lv L (2013) Acute ZnO nanoparticles exposure induces developmental toxicity, oxidative stress and DNA damage in embryo-larval zebrafish. Aquat Toxicol 136:49–59

Figures

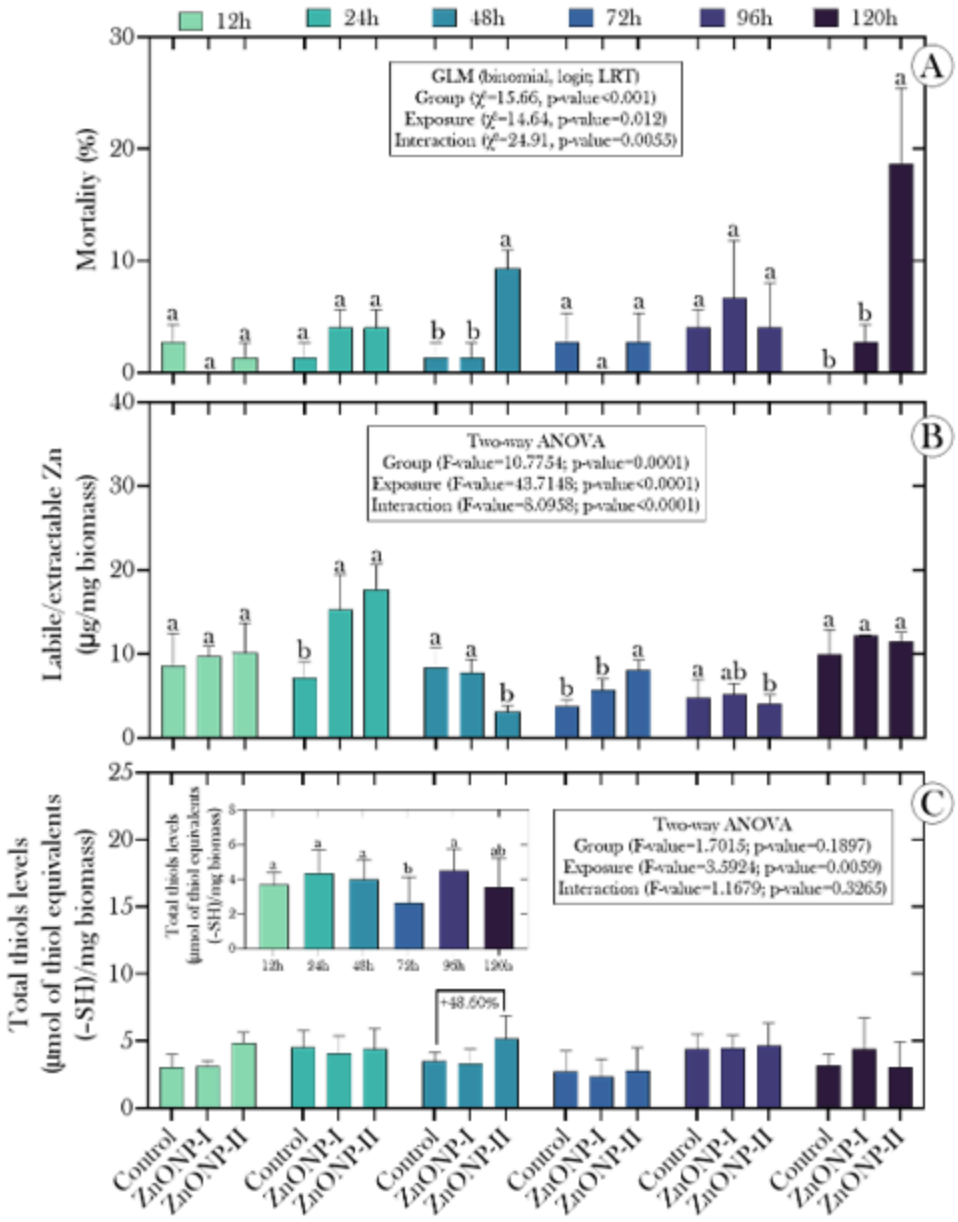


Figure 1

(A) Mortality rate, (B) labile/extractable Zn concentration, and (C) total thiol levels measured in adult *Tribolium castaneum* at different exposure times following dietary exposure to ZnO nanoparticles. Bars represent mean + standard deviation, and statistical summaries are displayed above each panel. Distinct lowercase letters indicate statistically significant differences among experimental groups within each evaluation time. ZnONP-I and ZnONP-II refer to dietary treatments containing 0.05% (500 mg kg^{-1}) and 0.2% (2000 mg kg^{-1}) ZnO NPs, respectively.

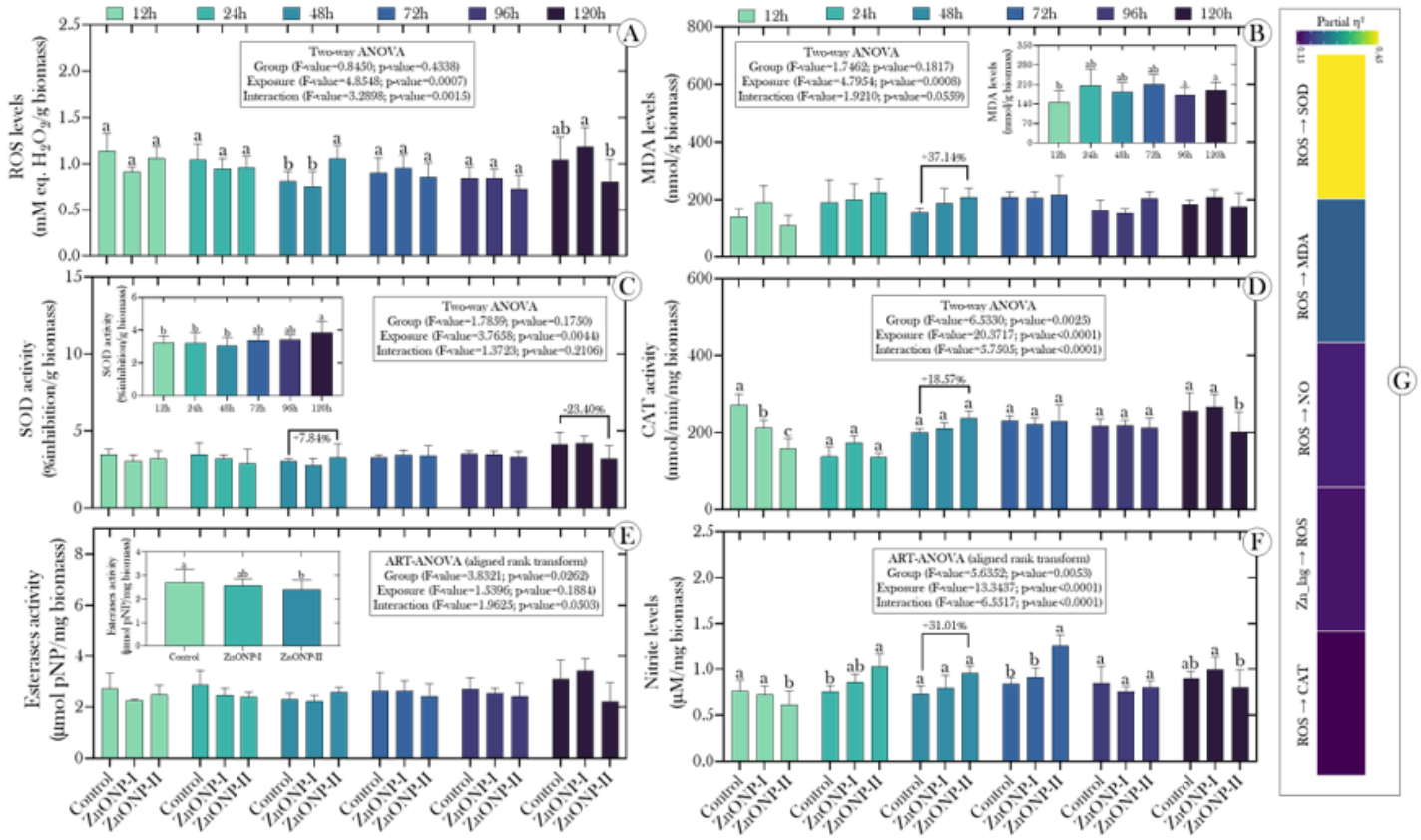


Figure 2

Oxidative and antioxidant responses of adult *Tribolium castaneum* following dietary exposure to ZnO nanoparticles across different exposure times. Panels show (A) reactive oxygen species (ROS), (B) malondialdehyde (MDA), (C) superoxide dismutase activity (SOD), (D) catalase activity (CAT), (E) esterase activity, and (F) nitrite levels (NO_2^-) as a proxy for nitric oxide production. Bars represent mean + standard deviation, and statistical summaries of the two-way ANOVA (or ART-ANOVA when assumptions were not met) are shown within each panel. Distinct lowercase letters indicate statistically significant differences among experimental groups within each exposure time. Panel (G) summarizes the hierarchical organization of the oxidative cascade, based on the effect sizes (partial η^2) derived from the sequential models presented in Table 1, illustrating the relative contribution of upstream drivers (Zn_lag →ROS) and downstream responses (ROS → SOD, ROS → MDA, ROS → NO, and ROS → CAT).

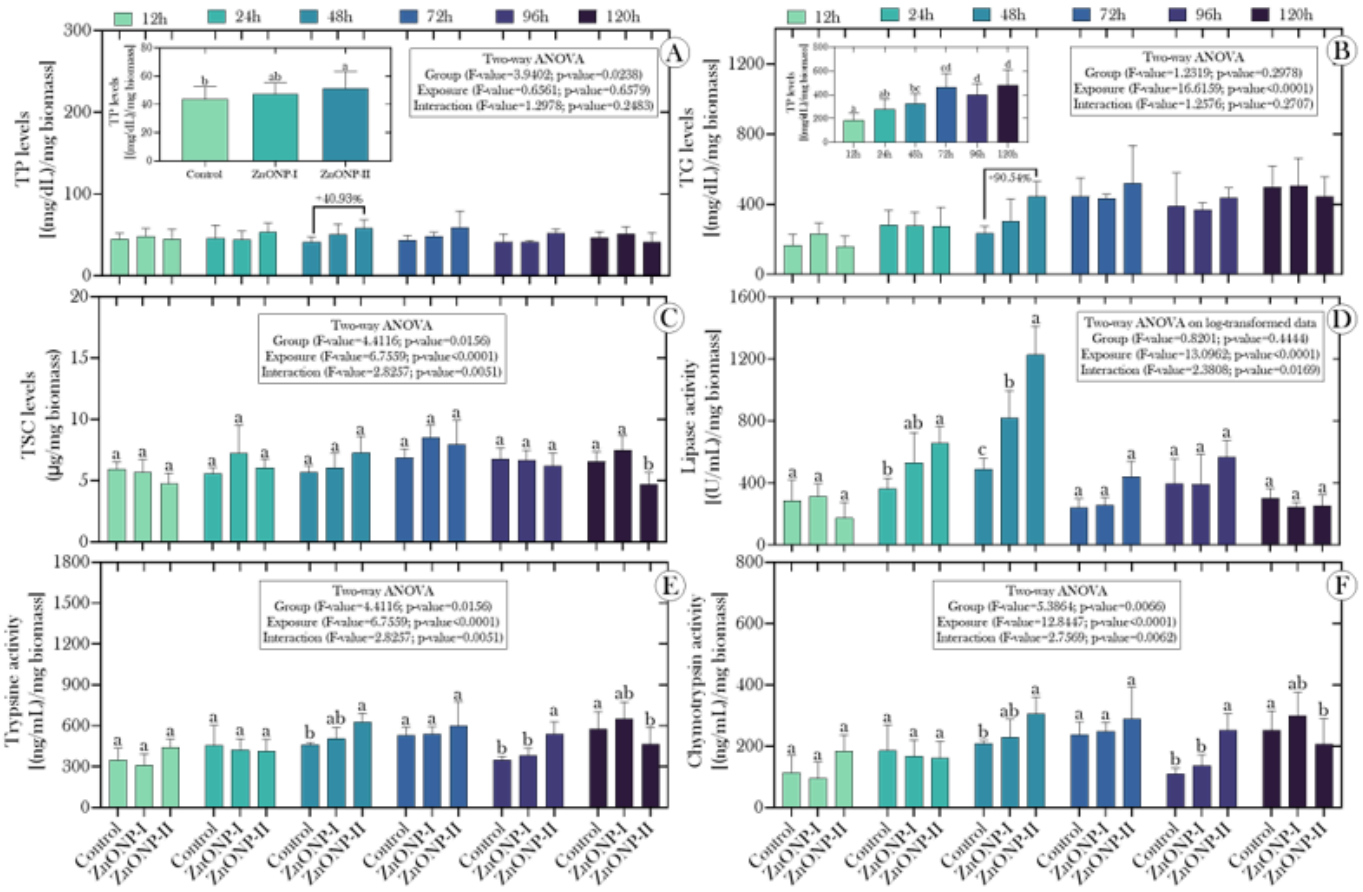


Figure 3

Metabolic and digestive responses of adult *Tribolium castaneum* following dietary exposure to ZnO nanoparticles across different exposure times. Panels show (A) total proteins (TP), (B) triglycerides (TG), (C) total soluble carbohydrates (TSC), (D) lipase activity, (E) trypsin activity, and (F) chymotrypsin activity. Bars represent mean + standard deviation, and statistical summaries of the two-way ANOVA are shown within each panel (ANOVA performed on log-transformed data in panel D). Distinct lowercase letters indicate statistically significant differences among experimental groups within each exposure time. ZnONP-I and ZnONP-II refer to dietary treatments containing 0.05% (500 mg kg^{-1}) and 0.2% (2000 mg kg^{-1}) ZnO nanoparticles, respectively.

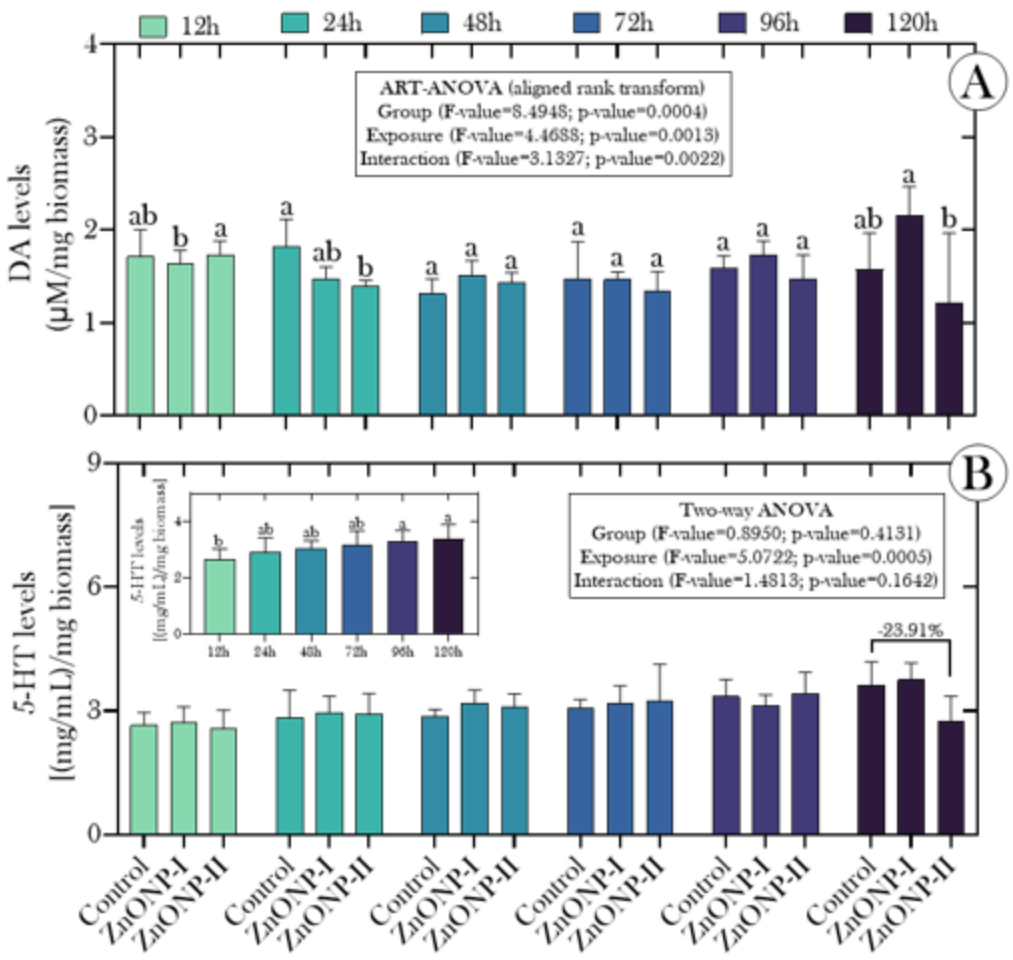


Figure 4

Neurochemical responses of adult *Tribolium castaneum* following dietary exposure to ZnO nanoparticles across different exposure times. Panels show (A) serotonin levels and (B) dopamine levels measured in insects. Bars represent mean + standard deviation, and statistical summaries of the models are shown within each panel. Distinct lowercase letters indicate statistically significant differences among experimental groups within each exposure time. ZnONP-I and ZnONP-II refer to dietary treatments containing 0.05% (500 mg kg^{-1}) and 0.2% (2000 mg kg^{-1}) ZnO nanoparticles, respectively.

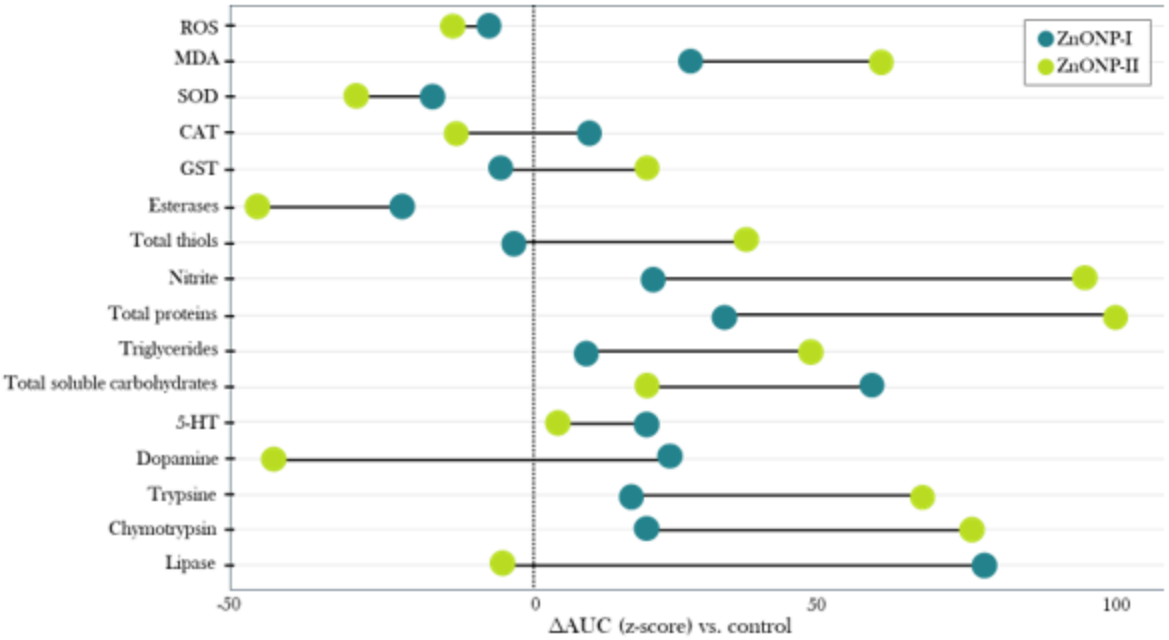


Figure 5

Standardized cumulative divergence of physiological biomarkers in *Tribolium castaneum*adults following dietary exposure to ZnO nanoparticles. Each point represents the standardized cumulative deviation from the control trajectory (ΔAUC), calculated as the area under the curve (AUC) for each biomarker over the entire experimental period (12–120 h). Positive values indicate sustained upregulation, whereas negative values indicate persistent suppression relative to the control condition. Blue and green points represent the ZnONP-I and ZnONP-II treatments, respectively. Biomarkers are organized along the vertical axis to illustrate the direction and magnitude of the integrated physiological deviation induced by each exposure scenario, highlighting the broader systemic divergence associated with the higher nanoparticle treatment.

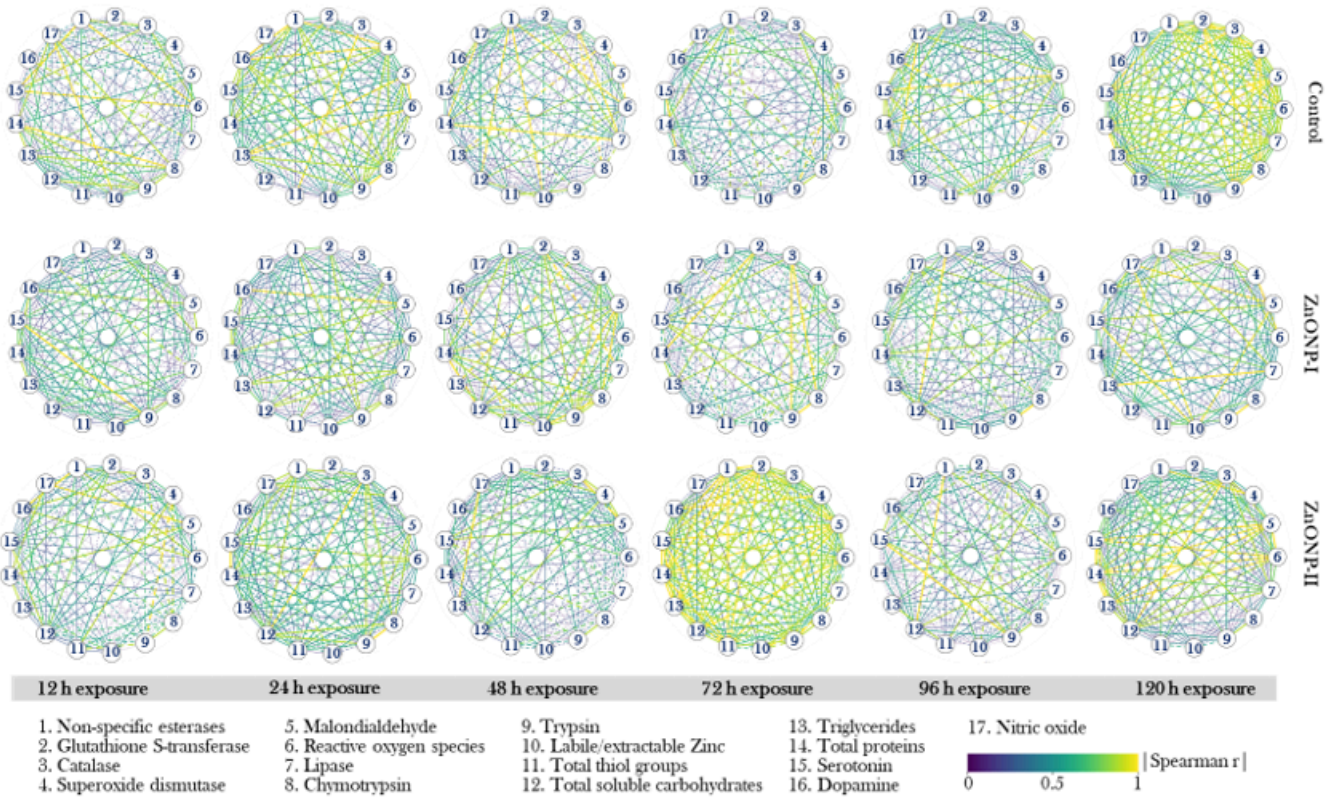


Figure 6

Temporal reorganization of biochemical interaction networks in *Tribolium castaneum*under dietary exposure to ZnO nanoparticles. Network diagrams represent the pattern of significant associations among biochemical biomarkers across exposure times (12, 24, 48, 72, 96, and 120 h). Each node corresponds to a biomarker (n = 17), and edges represent significant pairwise associations between biomarkers. Edge color reflects the strength of the association according to the color scale (from weak to strong interactions). Networks are arranged by treatment (rows) and exposure time (columns): the top row corresponds to the control group, the middle row to ZnONP-I, and the bottom row to ZnONP-II. The network observed for the ZnONP-II group at 72 h shows a marked increase in connectivity and interaction strength, consistent with the peak in network density and integration reported in Table 3, indicating a transient systemic reorganization of biochemical interactions under higher nanoparticle exposure.

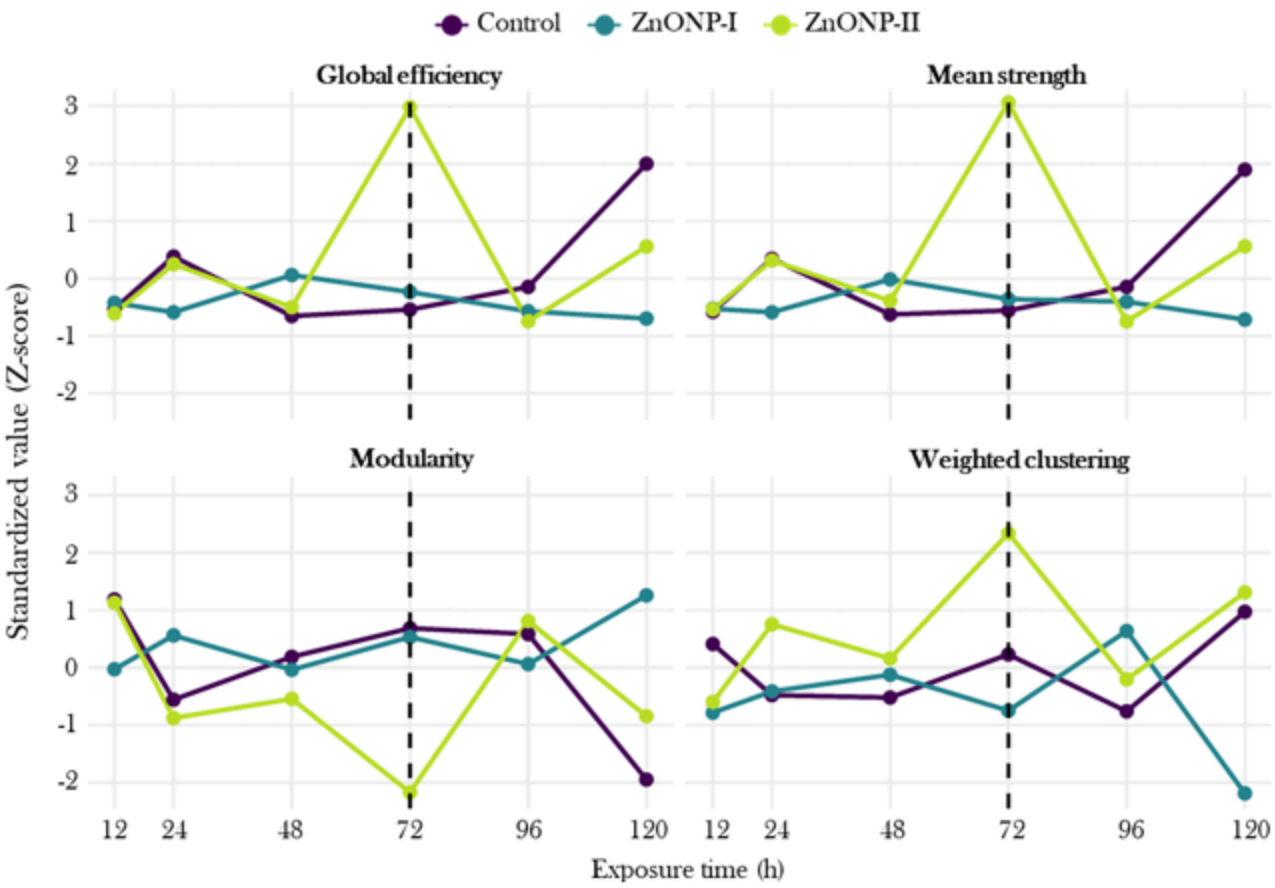


Figure 7

Temporal dynamics of topological metrics describing biochemical network organization in *Tribolium castaneum* under ZnO nanoparticle exposure. Panels show the temporal trajectories of key network properties calculated for the biochemical interaction networks: network density, weighted clustering coefficient, modularity, and mean connection strength. Lines represent the different experimental groups (Control, ZnONP-I, and ZnONP-II) across exposure times (12–120 h). The dashed vertical line highlights the 72 h exposure time, corresponding to the point of maximum network integration observed for the ZnONP-II group.

Supplementary Files

This is a list of supplementary files associated with this preprint. Click to download.

- SHORTABSTRACTTOC.docx